The 14th World Conference on Earthquake Engineering
October 12-17, 2008, Beijing, China

STEEL BAR FRACTURE OF REINFORCED CONCRETE FRAME UNDER EXTREMELY STRONG GROUND MOTION

Motoo SAISHO

Professor, Dept. of Architecture, Graduate School of Science and Technology, Kumamoto Univ., Kumamoto, Japan
Email: saisho@gpo.kumamoto-u.ac.jp

ABSTRACT:
The damage ratio equation of reinforced concrete member (RC-member) under strong cyclic load is derived on the basis of the very low-cycle fatigue of the steel bars. By applying the damage ratio equation to the column and beam composing RC-frame, the damage analysis method of multi-story RC-frame under extremely strong ground motion is proposed. Seismic response damages of multi-story RC-frames designed under variable design conditions are calculated by the presented numerical analysis method. From the calculated results, the effects of design conditions on the damage of RC-frame are investigated and it is shown that the steel bar fracture of RC member is closely related to the reinforcement ratio of it and the column-over-design factor of RC frame.

KEYWORDS: *reinforced concrete frame, seismic response analysis, steel bar fracture, low-cycle fatigue, damage ratio*

1. INTRODUCTION

Ultimate earthquake resistant capacity of multi-story frame is related to the ductility of the members composing the frame. The ductility of reinforced concrete member (RC-member), even if it is well designed to prevent the brittle shear failure, is effected by the fracture of longitudinal steel bar. The fracture test of RC-member under strong cyclic load has been carried out[1)-3)] and the steel bar fracture of RC-member is analytically investigated here. Basing on the test results it is pointed out that the steel bar fracture of RC-member under strong cyclic load is considered as the very low-cycle fatigue behavior[3)-4)]. The failure condition and the damage ratio equation of RC-member defined by steel bar fracture are also derived on the basis of the Coffin-Manson expression and the Palmgren-Miner rule[5)]. By introducing the failure condition of RC-member, the numerical analysis method of seismic response damage of multi-story RC-frame is derived[3)]. The damages of RC-frame under extremely strong ground motion are also examined by the proposed analysis method in relation with the structural design condition of it.

2. STEEL BAR FRACTURE TEST OF RC-MEMBER UNDER STRONG CYCLIC LOAD

2.1 RC-column specimen

The specimens are the cantilever RC-members shown in Fig.1. Fig.2 shows the loading conditions of them. Table-1 and Table-2 explain the test conditions and the material properties of reinforcing steel respectively. In Table-1, the specimens whose names are expressed by adding N at the end are the RC-columns to give the restoring force model and did not fracture. All specimens are fully reinforced by transverse reinforcement to prevent the shear failure of column. The concrete strength, the reinforcement ratio, the axial force, the loading rate and the amplitude of cyclic deformation are different among the specimens and the effects of them on the steel bar fracture of RC- column have been examined.

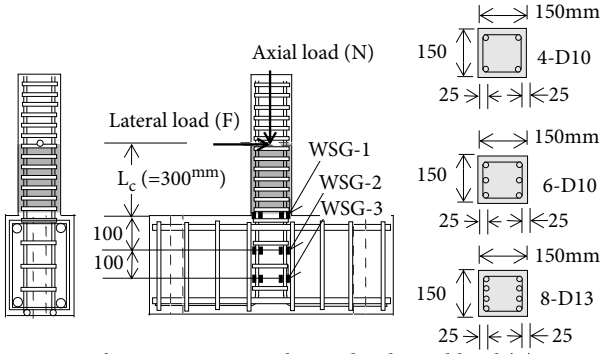

Fig.1 RC-column specimen subjected to lateral load (F) and varying axial load (N) simultaneously

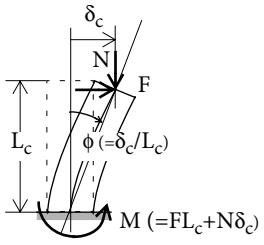

Fig.2 Loads of RC-column (F, N) and restoring force (M) of fixed-end

Table-1 Specimens and test results

Specimen	Load	δ_m/L_c	N_o/N_y	Reinforcement	$p_t^{(\%)}$ (= p_c)	$p_w^{(\%)}$	σ_c	$\varepsilon_{cu}^{(\%)}$	$(N_f)_{Test}$	$(N_f)_{Cal}$
SCDI-L-15	D I	0.15	0.15	6-D10	0.95	2.29	42.9	0.47	10.5	10.5
SCDI-L-20A	"	"	0.20	"	"	"	44.3	0.53	12.5	13.5
									13.5	
SCDI-L-20B	D I	0.15	0.20	6-D10	0.95	2.29	42.9	0.47	13.5	14.5
SCDI-L-20C	"	"	"	"	"	"	31.3	0.42	14.0	17.5
									17.0	
SCDI-L-30A	D I	0.15	0.30	6-D10	0.95	2.29	42.9	0.47	11.0	11.0
SCDI-L-30B	"	"	"	"	"	"	"	"	9.5	14.5
SCDI-L-40	"	"	0.40	6-D10	0.95	"	44.3	0.53	9.0	10.0
SCDI-S-15	"	0.20	0.15	8-D13	2.26	3.20	112.3	0.38	8.0	8.5
									9.0	
									9.5	9.5
SCDR-L-10	D R	0.11	0.10	6-D10	0.95	2.29	31.3	0.42	34.0	26.5
									50.5	
									77.5	
SCDR-L-20	D R	0.12	0.20	6-D10	0.95	2.29	31.3	0.42	35.0	30.5
SCSR-S-15N	S R	-	0.15	8-D13	2.26	3.20	112.3	0.38	-	-
SCSI-L-20N	S I	-	0.21	4-D10	0.63	1.26	32.3	0.53	-	-
SCSR-L-30N	S R	-	0.33	4-D10	0.63	1.60	35.8	0.46	-	-
SCDI-L-20N	D I	-	0.20	4-D10	0.63	1.60	29.7	0.49	-	-
SCDI-L-30N	"	-	0.30	6-D10	0.95	"	38.7	0.56	-	-
SCDR-L-30N	D R	-	"	4-D10	0.63	"	35.8	0.46	-	-

Notation of specimen
SCDI- L-15
1 2 - 3 - 4

1: RC short column (Column length (L_c)=300mm)
2: Time history of column deformation
(I: Sinusoidal wave of incremental amplitude, R: Random wave)
3: Concrete strength(L, S)
(S: Super-high strength, L: Ordinary strength)
4: Initial axial force ratio (N_o/N_y)

δ_m : Maximum lateral deformation
p_t : Tension reinforcement ratio
p_c : Compression reinforcement ratio
p_w: Hoop reinforcement ratio
σ_c : Compression strength of concrete (N/mm^2)
ε_{cu}: Ultimate strain of concrete
$(N_f)_{Test}$: Tested cycles to fracture
$(N_f)_{Cal}$: Calculated cycles to fracture

Table-2 Material properties of steel bar

Reinforcement	σ_y	σ_u	$\varepsilon_y^{(\%)}$	$\varepsilon_f^{(\%)}$
D10	370	547	0.192	23.9
D13	417	684	0.189	22.7

σ_y : yield stress (N/mm^2)
(=P_y/A_s, P_y: yield axial force, A_s: sectional area)
σ_u : tensile strength (N/mm^2)
(=P_u/A_s, P_u: ultimate axial force)
ε_y : yield strain
ε_f : fracture strain (obtained at 0.90σ_u)

2.2 Loading conditions

The cantilever RC-members are subjected to axial load (N) and lateral load (F) as explained in Fig.2. To simulate the seismic response behavior of RC-member, the reversed cyclic lateral load (F) and the varying axial load (N) were applied dynamically. The lateral load and the axial load varied independently with time and there was no relation between them. In the dynamic loading test the maximum velocity of lateral deformation at the loading point was nearly 100mm/second and the maximum strain rate of the longitudinal steel bar was about 0.1/second -0.3/second.

2.3 Steel bar fracture of specimen

The steel bar fracture of every specimen was obtained by the steel bar strains, which were measured by the wire strain gages (WSG-1, WSG-2, WSG-3) attached to the longitudinal steel bars shown in Fig.1. The time histories of the steel bar strains measured by WSG-3 and the deformation are shown in Fig.3 in which the fracture point of steel bar is designated by the dashed line. The strain of steel bar which did not fracture is also shown in Fig.3(C) to compare with the strain of fractured steel bar in Fig.3(B). When the steel bar fractured, the steel bar strain decreased suddenly and remarkably (Fig.3(B)) even if the direction of incremental deformation (δ_c) did not change (Fig.3(A)). Furthermore, the restoring force deteriorated suddenly when the steel bar fractured as shown in Fig.3(D). From the behaviors observed in Fig.3, the following conditions are assumed to be satisfied simultaneously to decide the steel bar fracture of every specimen.

i) Steel bar strain decreases suddenly and remarkably. After that the steel bar strain does not increase again.

ii) The steel bar is subjected to the tension reinforcement force.

iii) The direction of incremental deformation of specimen does not change.

The test results are shown in Table-1 in which $(N_f)_{Test}$ is the number of cycle of plastic strain when the steel bar fractured. In the decision of $(N_f)_{Test}$, regardless of the variable amplitude of cyclic strain of steel bar, only the cycles whose peak-to-peak amplitudes are larger than $2\varepsilon_y$ (ε_y : yield strain) are counted in. The loading of every specimen stopped just after the first fracture of steel bar was

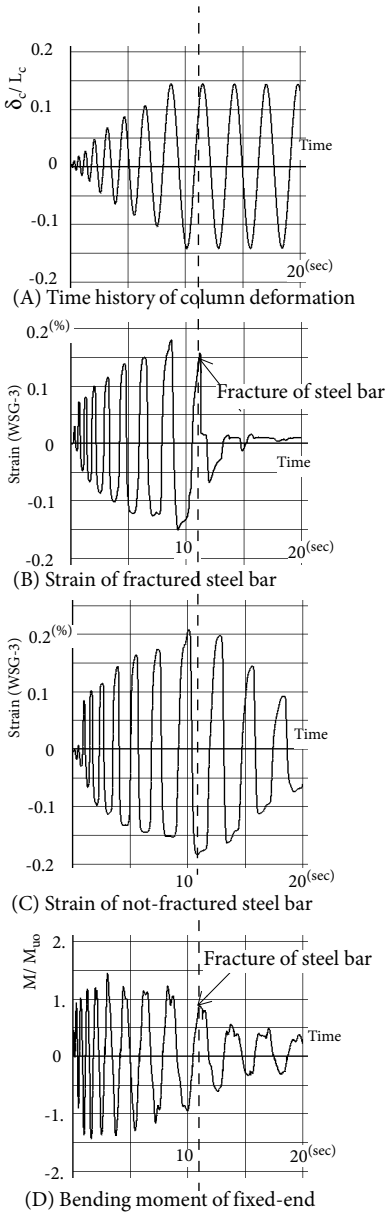

Fig.3 Time history of steel bar strain to show the steel bar fracture (SCDI-L-20C)

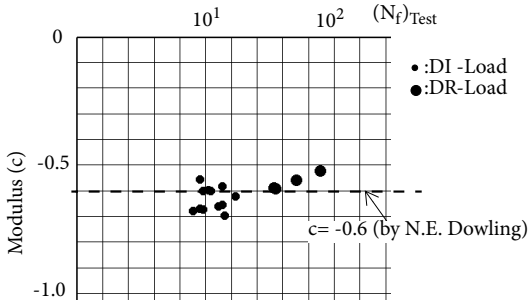

Fig.4 Modulus (c) of Coffin-Manson expression when the calculation coincides with test result

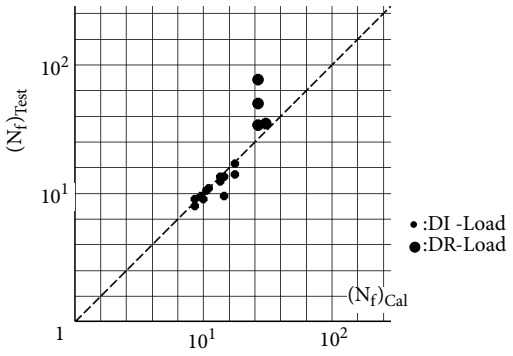

Fig.5 Comparison of calculated steel bar fracture by the very low-cycle fatigue and test result

observed by the video recorder and the fracture sound. From this reason the 16 steel bars among the 31 longitudinal steel bars under the same loading condition fractured and the other steel bars (15 steel bars) did not fracture. Accordingly the test results shown in Table-1 are corresponding to the lower limit of steel bar fracture.

3. ANALYSIS OF STEEL BAR FRACTURE AND FAILURE OF RC-MEMBER

3.1 Analysis of steel bar fracture

In this study the steel bar fracture under strong seismic load is assumed to be the very low-cycle fatigue and the analysis method of steel bar fracture of RC-member is derived on the basis of the Coffin-Manson expression and the Palmgren-Miner rule. According to the Coffin-Manson expression the number of cycles until the steel bar fractures (N_f) is expressed by the plastic strain amplitude (ε_{pa}) as shown in Eq.(1).

$$\varepsilon_{pa} = \varepsilon_f (2N_f)^c \qquad (1)$$

in which ε_f: fracture strain, c: constant. The number of cycle to fracture (N_f) of the Coffin-Manson expression is defined under the cyclic load whose amplitude is constant. In this study it is assumed that the Coffin-Manson expression is applicable to the steel bar fracture under the cyclic load of varying amplitude and the damage of each cycle is approximated by $1/N_f$. The damage ratio of steel bar fracture ($_sD_{cr}$) at any moment under cyclic load is given by the summation of damage of every cycle and expressed by Eq.(2) in which N_{fj} means the number of cycle to fracture under the j-th cycle load.

$$_sD_{cr} = \sum_j \frac{1}{N_{fj}} \qquad (2)$$

The fracture condition of steel bar is given by $_sD_{cr}=1$.

The modulus (c) in Coffin-Manson expression (Eq.(1)) is obtained under the condition that the predicted fracture coincides with the fracture of test and shown in Fig.4. As shown in Fig.4, the calculated values are nearly constant and satisfy the assumption of Coffin-Manson expression that the modulus (c) is constant. These results show that the analysis method derived in this study is useful to analyze the steel bar fracture of RC-member. In this paper the value of modulus (c) is given by c= -0.6 which is approximated by the average in Fig.4 and coincides with the value presented by N.E. Dowling[5]. The calculated cycles to fracture $(N_f)_{Cal}$ of each specimen are shown in Table-

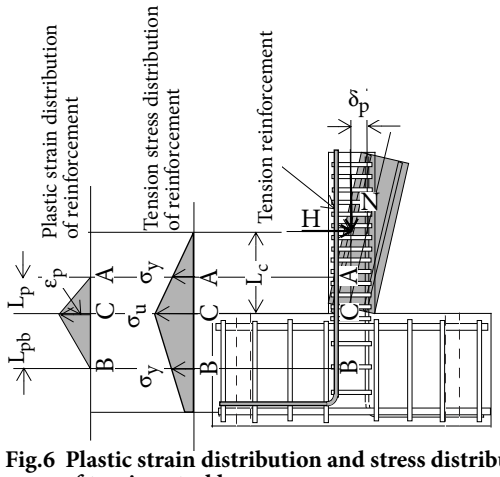

Fig.6 Plastic strain distribution and stress distribution of tension steel bar

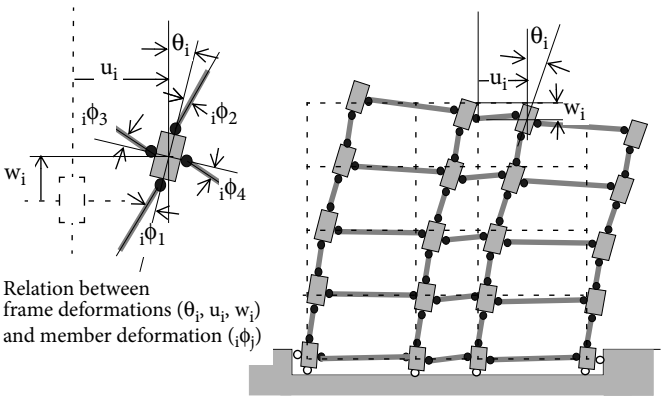

Fig.7 Frame model of numerical analysis

1. They are compared with test results in Fig.5 and show a good correlation with test results.

In order to apply the fracture equation of steel bar mentioned above to the analysis of the seismic response damage of multi-story RC-frame, the plastic strain of steel bar in Eq.(1) need to be given by the deformation of members. To express the relation of the plastic strain of steel bar (ε_p) and the plastic deformation of RC-member (δ_p), the plastic strain of steel bar is approximated to distribute linearly in relation with the stress distribution as shown in Fig.6. From these conditions, the plastic strain is expressed by Eq.(3).

$$\varepsilon_p=\{(D-d-x_n)/\Lambda\}\delta_p \quad \text{(Left side longitudinal steel bar)},$$
$$\varepsilon_p=\{(d-x_n)/\Lambda\}\delta_p \quad \text{(Right side longitudinal steel bar)} \qquad (3)$$

in which $\Lambda=(3L_c-L_p)L_p/6+L_{pb}L_c/2$, L_c: column length, L_{pb}, L_p: plastic zone length of steel bar, D: depth of column section, d: depth of cover concrete, x_n: distance of neutral axis from the right side edge of column section as shown in Fig.6. By the use of Eq.(3), the plastic deformation of RC-member (δ_p) is transformed to the plastic strain of steel bar (ε_p). The amplitude of the plastic strain of steel bar (ε_{pa}) is given by the peak-to-peak strain of the cyclic plastic strain under seismic load. Substituting the plastic strain amplitude ε_{pa} (Eq.(3)) in Eq.(1) and Eq.(2), the damage ratio of steel bar ($_sD_{cr}$) under seismic load can be calculated.

4. NUMERICAL ANALYSIS OF SEISMIC RESPONSE DAMAGE OF MULTI-STORY RC-FRAME

4.1 Multi-story frame model

Multi-story RC-frames are numerically analyzed. They are composed of the rigid beam-column connections and the axially elastic members with elastic-plastic hinges at the both ends as explained in Fig.7. The restoring force of the elastic-plastic hinge is corresponding to the fixed-end moment M (=F L_c+N δ_c) shown in Fig.2 and expressed by the dynamic restoring force model explained in the next section. The damage of the elastic-plastic hinge of RC-member is expressed by the steel bar fracture ratio (Eq.(2)). The mass of frame is concentrated in every beam-column connection and distributed uniformly in it. The deformation of frame is expressed by the rotation (θ_i, i: number of beam-column connection), the horizontal displacement (u_i) and the vertical displacement (w_i) of every rigid beam-column connection.

4.2 Dynamic restoring force model of RC-member

The restoring force model of the elastic-plastic hinge of multi-story frame was derived from the fixed-end moment M(=F L_c+N δ_c) of cantilever RC-member under lateral load (F) and axial load (N) shown in Fig.2. Based on the cyclic loading test of cantilever RC-member, the dynamic restoring force (M) of elastic-plastic hinge is approximated by superposing the varying axial force effect and the loading rate effect on the static restoring force under constant axial force.

4.2.1 Static restoring force model

The load deformation relations of static test[1)-3)] are shown with thick lines in Fig.8. In these figures the restoring force M(=F L_c+$N_o\delta$) is the bending moment at the fixed-end of column. M_{uo} is the ultimate bending moment under constant axial force (N_o). The ultimate bending moment is calculated under the following conditions.

i) The maximum compression strain of concrete in the section is just equal to the ultimate compression strain of concrete (Table-1).

ii) The stress-strain relation of concrete is assumed to be expressed by the Bi-linear model whose plastic strength is given by the compression strength of concrete (σ_c). The stress-strain relation of reinforcing steel is also assumed to be expressed by the Bi-linear model whose plastic strength is equal to the yield stress (σ_y). It is shown in Fig.8 that M_{uo} can predict well the maximum bending moment of the specimen under static load and the calculation method of it mentioned above is also useful. In Fig.8 the restoring force expressed by the modified Clough model (Clough model[6)]) is shown by the thin lines. The test results are well predicted by the Clough model. In this study the basic restoring force model (BRF model), which is corresponding to the static restoring force under constant

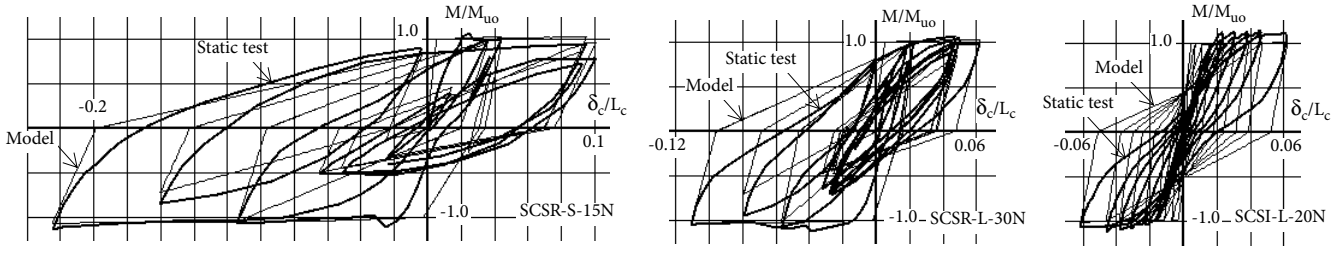

Fig.8 Load-deformation relations of RC-column under static horizontal load and constant axial load

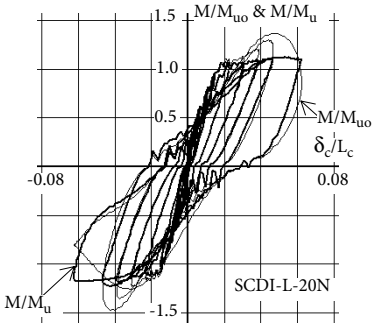

Fig.9 Restoring force characteristics under varying axial force

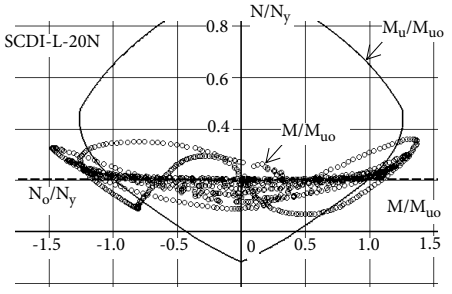

Fig.10 N-M relations of dynamic loading test compared with the calculated relation

axial force, is expressed by the Clough model. The BRF model and its skeleton curve are explained in Fig.12.

4.2.2 Varying axial force effect on restoring force of fixed-end moment of RC-member

The varying axial force effect[2] on the restoring force of fixed-end moment of cantilever RC-member is explained in the load-deformation relations in Fig.9 and the N-M relation in Fig.10. The thin line in Fig.9 shows the fixed-end moment of the specimen (M) divided by M_{uo} which is the ultimate bending moment under the initial axial force (N_o). The load-deformation curve (M/M_{uo}-δ_c/L_c) in Fig.9 is very complicated and changes according to the varying axial force (N). The effects of the varying axial force on the bending moment of specimen (N-M relation) are explained in Fig.10. In Fig.10 it is shown that the bending moment (M) is nearly equal to the calculated ultimate bending moment (M_u) under the axial force at that moment in the plastic range of deformation. Accordingly the effect of varying axial force can be modeled by the use of the restoring force divide by M_u (M/M_u).

The thick line in Fig.9 shows the restoring force divide by M_u. We can see that the thick line to express M/M_u is nearly constant in the plastic range and fairly regular comparing with the thin line to show M/M_{uo}.

4.2.3 Loading rate effect on restoring force of RC-member

To express the loading rate effect on the restoring force of RC-member, whose loading rate varies irregularly at every moment, the r-value defined by Eq.(4) is introduced in this study.

$$r = ({}_dm - {}_sm)/{}_sm \qquad (4)$$

in which ${}_dm$, ${}_sm$ are the ratios of dynamic and static restoring force to the calculated ultimate bending moment (M/M_u) under the same hysteretic deformation. The values of ${}_dm$, ${}_sm$ are defined by the restoring force from the last reversal point of the cyclic load as explained in Fig.11. The dynamic and static loading tests of RC-member under the same cyclic deformation have been carried out[2] and Eq.(5) to give the r-value is obtained from them.

$$1/r = C_1 d_A + C_2 |d_B| + C_3 \qquad (5)$$

in which d_A is the accumulated plastic deformation ratio ($=\Sigma|\Delta\phi_p|/\phi_u$, $\Delta\phi_p$: incremental plastic deformation, Σ: summation of increments) and d_B is the plastic deformation ratio (ϕ_p/ϕ_u) from the last reversal point as shown in Fig.11. In Eq.(5) the parameters C_1, C_2, C_3 are the constants which are not effected by the cyclic deformation, the velocity of deformation and loading conditions. On the basis of the test result, the most suitable parameters C_1, C_2, C_3 to predict the test results by Eq.(5) are obtained[2] and shown in Table-3. By the use of r-value given by Eq.(5), the loading rate effect on the restoring force of RC-member under dynamic load can be predicted.

4.2.4 Dynamic restoring force model and dynamic loading test

By superposing the loading rate effect and the varying axial force effect on the BRF model, which is corresponding to the static restoring force model under constant axial force, the dynamic restoring force under varying axial force is obtained. To superpose the loading rate effect and the varying axial force effect on the BRF model is carried

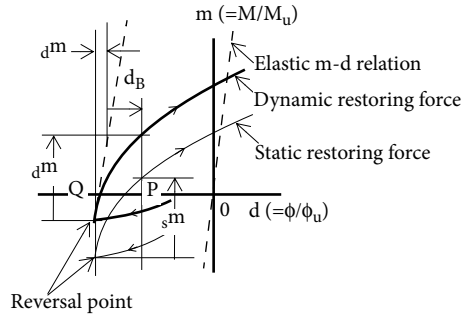

Fig.11 Definitions of the restoring force ratio (${}_dm$, ${}_sm$) and the deformation ratio (d_B) from the reversal point (Q)

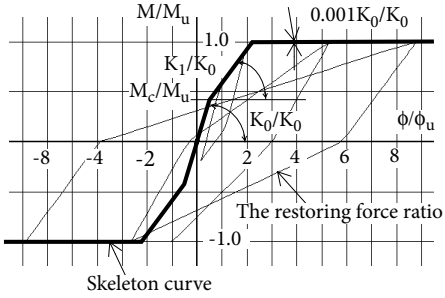

Fig.12 Basic restoring force model (BRF model) and its skeleton curve

out by the use of Eq.(5) and the restoring force divide by M_u (M/M_u). The presented method to express the dynamic restoring force under varying axial force is comparatively simple and can be applied to the numerical seismic response analysis. The dynamic restoring forces by the presented method are shown in Fig.13 comparing with the dynamic loading test under varying axial force. It is shown in Fig.13 that the dynamic restoring force model predicts well the complicated hysteretic curves and the maximum restoring forces.

4.3 Design conditions of multi-story RC-frame

For the numerical analysis RC-frames are designed under the following conditions.

i) The frame strengths are defined by the base shear strength ratio (C_B). The strengths of 10-story frame and 5-story frame are C_B=0.30 and C_B=0.45 respectively. They are calculated by the limit analysis assuming the collapse mechanism of frame with plastic hinges at every beam-end and every column-end of first and top story.

ii) The distribution of story-shear strength ratio is equal to that given in the Japanese design code.

iii) The column-over-design factor (r_c) of every beam-column connection except the top story is the same in each frame. The factors of designed RC-frame are r_c=1.0, 1.5.

iv) The longitudinal reinforcement ratio p_t (=p_c) of every column and beam is the same in each frame. The ratios of designed RC-frame are p_t=0.5%, 1.0%, 1.5%.

v) The width-to-depth ratios (b/D) of column and beam of every frame are b/D=1.0 and b/D=1/2 respectively.

Multi-story RC plane frames analyzed in this study are 10-story 3-span frame and 5-story 3-span frame. Every story height is 4.0 m and the span lengths of outer span and inner span are 8.0 m and 6.0 m respectively. The weight of each story is 2000KN. In the design of these RC-frames, the compression strength of concrete (σ_c) is assumed to be σ_c= 50N/mm^2. The yield stress (σ_y) and tensile strength (σ_u) of steel bar are σ_y=340N/mm^2, σ_u=440N/mm^2.

4.4 Ground motion

To calculate the seismic response damage of RC-frame, JMA-KOBE NS & UD (1995) recorded in Kobe and the artificial ground motion (ART NS & UD) are used as input ground motion. The acceleration response spectra (S_a) of them are shown in Fig.14 comparing with each others. In order to investigate the effect of the characteristics of ground motion, the ground motions satisfy the conditions that the spectrum intensities (SI) of them are the same and the response spectra are quite different between them.

5. CALCULATED SEISMIC RESPONSE DAMAGE OF RC-FRAME

The seismic response damages of RC-frame are calculated by the proposed analysis method. The maximum plastic deformation of every member (ϕ_m) and the damage ratio of steel bar fracture ($_sD_{cr}$) are shown in Fig.15-Fig.18. The values of ϕ_m and $_sD_{cr}$ are expressed by the thick lines perpendicular to the axis of column and beam. The thick lines are also explained by the numerals in the figures. The calculated results in Fig.15-Fig.18 show the following characteristics of the seismic response damage of RC-frame.

i) There are clear differences between the distributions of the maximum plastic deformation (ϕ_m) and the damage ratio of steel bar fracture ($_sD_{cr}$).

ii) The remarkable concentrations of damage ratio in some frames are observed even if the column-over-design factors (r_c) of them are large enough and they are designed well.

iii) The maximum damage ratio of RC-member is apparently effected by the column-over-design factor of RC-frame and the reinforcement ratio of member (p_t).

6. CONCLUSIONS

The steel bar fracture of RC-member under strong cyclic load has been tested and analyzed on the basis of the very low-cycle fatigue behavior. By introducing the fracture equation of steel bar, the numerical analysis method of

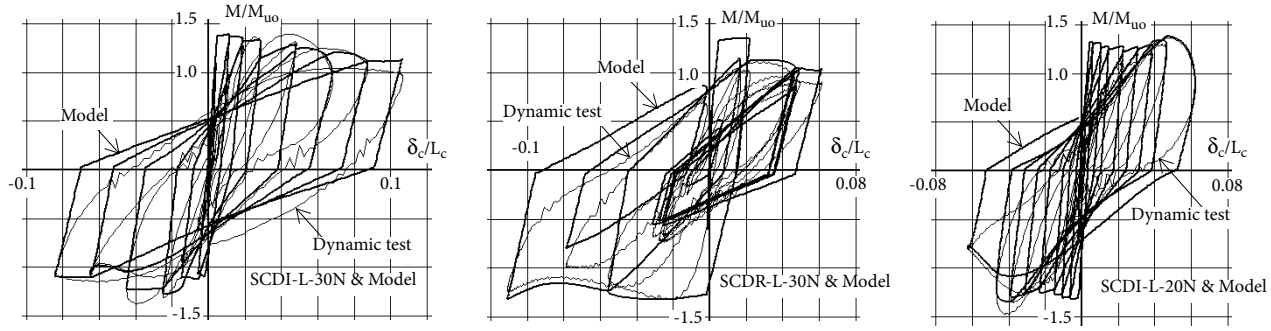

Fig.13 Dynamic restoring force of RC-column under varying axial load

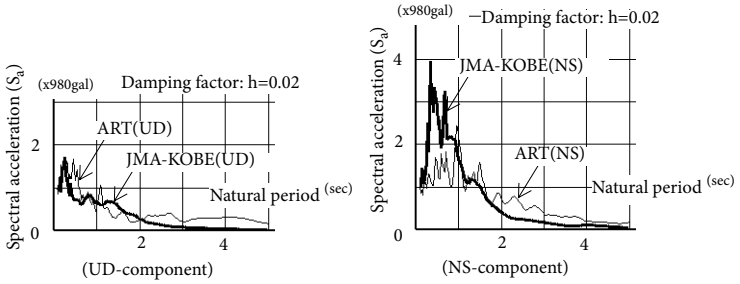

Fig.14 Response spectra of strong ground motion used in numerical analysis

Table-3 Parameters (C_1, C_2, C_3) in Eq.(5)

RC-column specimen (L_c/D)	C_1	C_2	C_3
Long column (4.67)	0.0431	0.1043	3.00
Short column (2.00)	0.0169	0.0433	3.00
Very short column (1.33)	0.0104	0.0281	3.00

the seismic response damage of RC-frame is also derived. From the calculated seismic response damages by the proposed analysis method, it is shown that the earthquake resistant design condition against steel bar fracture is different from that to prevent the concentration of plastic deformation of RC-frame.

REFERENCES

1) Saisho,M. and Suda,K., Restoring Force Model of RC Beam-Column Subjected to Dynamically Varying Axial Force, *Proceedings of the 12th World Conference on Earthquake Engineering*, Paper No.1024, 2000.1.

2) Saisho,M.and Hayamichi,D., Dynamic Restoring Force Model of RC-Column under Seismic Load, *Proceedings of the 13th World Conference on Earthquake Engineering* , Paper No.1867, pp.1-14, 2004.8.

3) Saisho,M., Hayamichi,D. and Toda,Y., Damage of Reinforced Concrete Structure under Extremely Strong Ground Motion, *Proceedings of the 13th European Conference on Earthquake Engineering* , Paper No.771, pp.1-15, 2006.9.

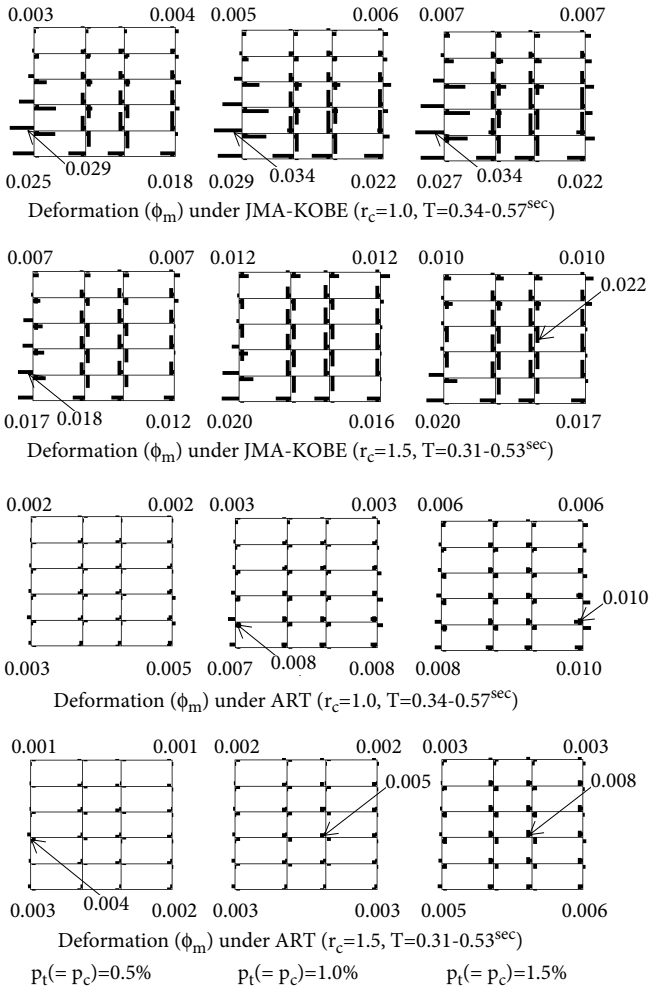

Fig.15 Seismic response deformation of 5-story RC-frames

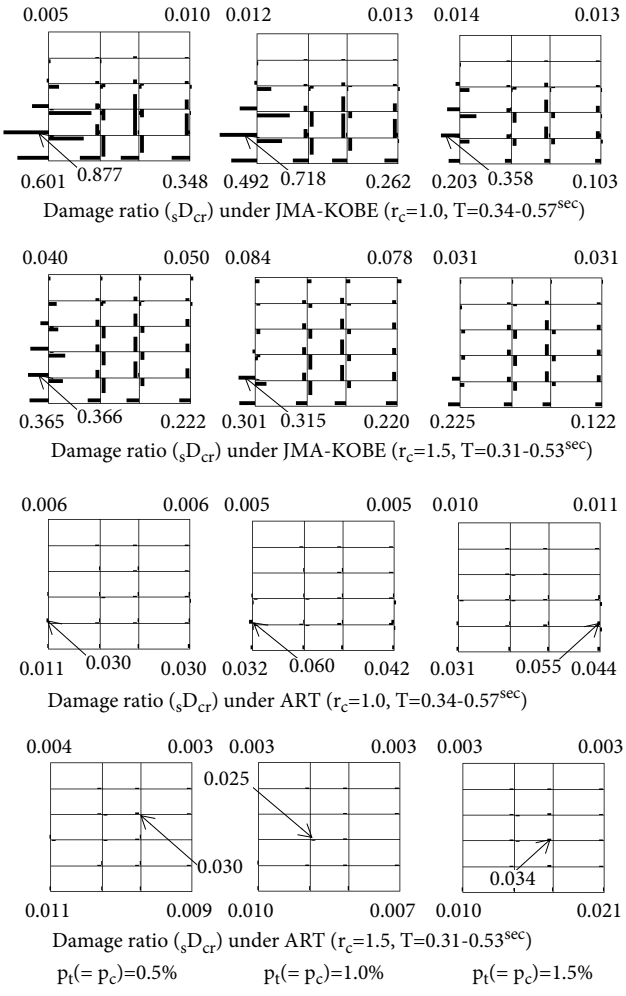

Fig.16 Seismic response damage of 5-story RC-frames

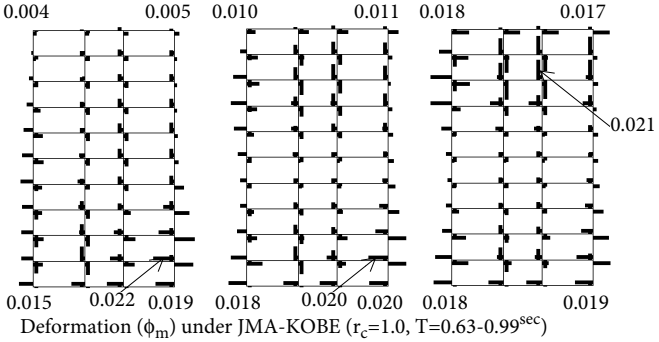

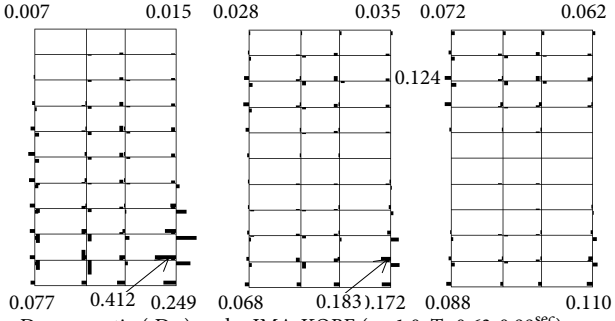

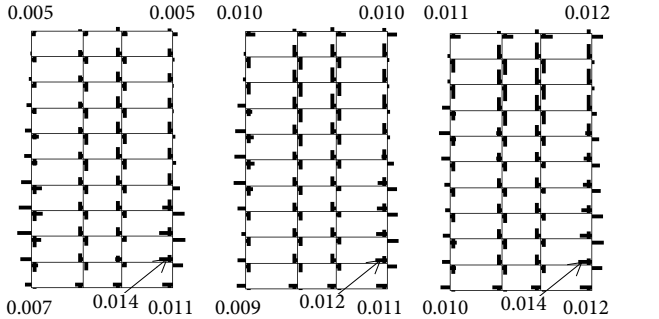

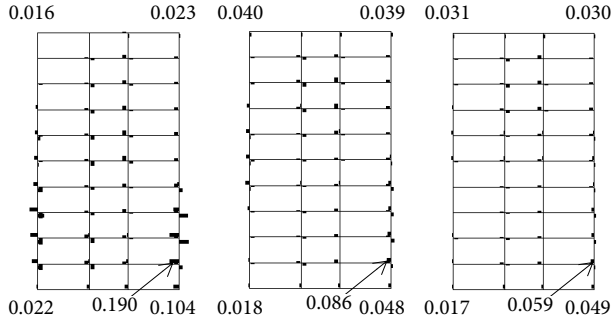

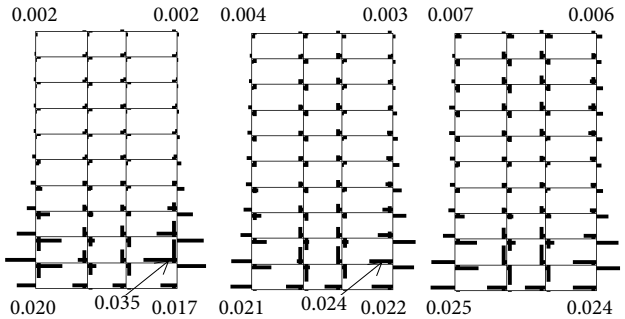

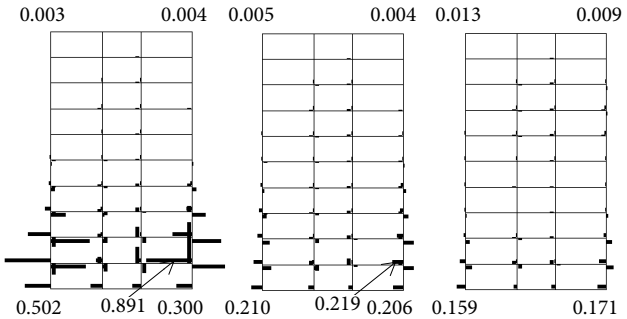

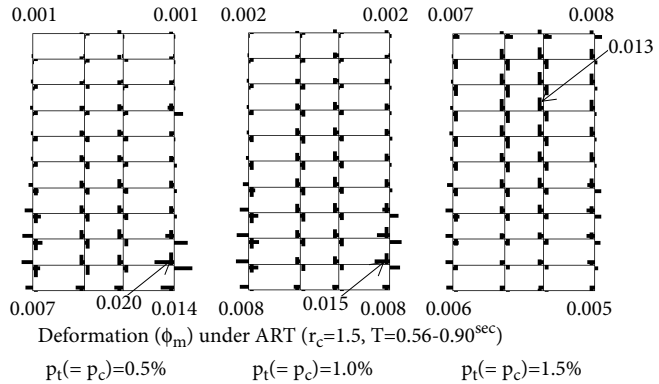

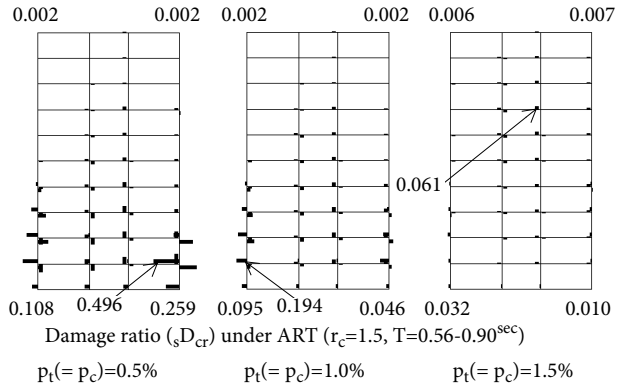

Fig.17 Seismic response deformation of 10-story RC-frames

Fig.18 Seismic response damage of 10-story RC-frames

4) Brown, J. and Kunnah, S.K., Low-Cycle Fatigue Failure of Reinforcing Steel Bars, *ACI Material Journal*, pp.457-466, 2004.11-12.

5) Dowling, N.E., Mechanical Behavior of Materials, *Prentice Hall*, 1993.

6) Clough, R.W. and Johnston, S.B., Effect of Stiffness Degradation on Earthquake Ductility Requirements, *Proceedings of Japan Earthquake Engineering Symposium*, pp.227-232, 1966.10.

Acknowledgement

This study was supported by the Grant-in-Aids for Scientific Research of Japan No.08455263, No.14550573, No.16560502 and No.20560526.